

Goniometric optical scatter instrument for out-of-plane ellipsometry measurements

Thomas A. Germer and Clara C. Asmail

Optical Technology Division

National Institute of Standards and Technology

Gaithersburg, Maryland 20899

ABSTRACT

A goniometric optical scatter instrument has been developed at the National Institute of Standards and Technology which can readily perform measurements of optical scatter and its associated polarization in directions out of the plane of incidence. This paper describes the coordinate transformations that are required to operate such a goniometer with respect to sample-specific coordinates. We present new methods for measuring the 3×3 non-handed Mueller matrix elements using dual rotating half-wave retarders, and present a subset of the Mueller matrix, referred to as the bidirectional ellipsometric parameters which have been shown to simplify the interpretation of the data. The results of out-of-plane Mueller matrix and bidirectional ellipsometric measurements from a titanium nitride layer on silicon are presented.

I. INTRODUCTION

Optical scattering has been shown to be a powerful diagnostic technique for characterizing optical quality surfaces.¹ The fundamental description of optical scattering can

be encapsulated in the bidirectional reflectance distribution function (BRDF), defined as the reflected radiance L_r normalized by the incident irradiance E_i , given by²

$$f_r(\theta_i, \phi_i; \theta_r, \phi_r) = L_r/E_i = (d\Phi_r/d\Omega)/(\Phi_i \cos \theta_r), \quad (1)$$

where $d\Phi_r/d\Omega$ is the reflected power per unit solid angle, Φ_i is the incident power, θ_r and ϕ_r are the polar and azimuthal angles of the reflected light, and θ_i and ϕ_i are the polar and azimuthal angles of the incident light. Although the BRDF is often reported as a polarization-averaged quantity, it should in fact be a Mueller matrix F_r , relating the reflected Stokes-radiance vector \mathbf{L}_r to the incident Stokes-irradiance vector \mathbf{E}_i :

$$\mathbf{L}_r = F_r \mathbf{E}_i. \quad (2)$$

Calculations, and recent experimental results, have demonstrated that a wealth of information is included in the polarimetric properties of surfaces.³⁻¹² Even more so, the polarimetric properties of scattering out of the plane of incidence can allow the distinction amongst different types of defects on smooth surfaces.^{6,7}

It is common to measure the light scattering properties of samples in directions within the plane of incidence, since this configuration requires the least hardware and is the easiest to construct. Instruments capable of out-of-plane measurements have been constructed, but tend to be large and much more difficult and expensive to fabricate, often since the source and detector are both expected to move.¹³ In this paper, we describe an automated scatterometer, capable of measurements out of the plane of incidence, which has a fixed source and a detector that rotates about a single axis.^{14,15} Rotation of the sample about three axes, and translational motion along two, is sufficient to fully select all possible incident/viewing direction combinations on any location on a sample. Much of the difficulty of the design of this instrument is not mechanical, but

rather conceptual, since one must know the transformation from the goniometer coordinates to the incident and scattering directions with respect to the sample and the inverse transformation.

In Sec. II, we describe the instrument. In Sec. III, the algorithms for converting between the goniometer coordinates and the sample coordinates are derived. Section IV describes procedures for performing polarimetric measurements of samples. Finally, in Sec. V, some experimental results of out-of-plane Mueller matrix measurements are presented.

II. DESCRIPTION OF THE INSTRUMENT

Figure 1 shows an overall schematic diagram of the goniometric optical scatter instrument. Light from one of three lasers, HeNe (wavelength $\lambda = 633$ nm), frequency-doubled Nd:YAG ($\lambda = 532$ nm), or HeCd ($\lambda = 442$ nm or 325 nm), passes through a power stabilizer, a chopper, a polarizer, a retarder (currently $\lambda/2$) mounted on a computer controlled rotation stage, a lens (focal length = 100 mm), and a pinhole (diameter = 50 μm), before being directed and focussed with a super-polished concave mirror (focal length = 230 mm) through the center of a goniometer. The light is focused to the solid-angle-defining aperture of a receiver.

Figure 2 shows a schematic diagram of the goniometer. It is a three-axis four-angle goniometer with α being the angle of rotation of the sample about a vertical axis, β being the angle of rotation of the sample about a horizontal axis which moves with α , γ being an angle of rotation about the sample azimuth (moving with α and β), and δ being the angle of rotation of the detector about the vertical axis. When $\alpha = \beta = \gamma = \delta = 0$, the sample is positioned so that the light is incident at normal incidence and the detector (if it were not blocking the incident light) is positioned to collect the specularly

reflected light. With this configuration nearly any combination of incident and scattering directions can be achieved, being limited only by obscuration of either the incident or scattered beam by the sample mount and β rotation stage (at angles $\theta > 87^\circ$ on one side of the sample and 65° on the other) or occultation of the incident beam by the receiver (within 5° of retroreflection).

Figure 3 shows a schematic of the receiver. A computer-controlled translation stage selects one of three solid-angle-limiting apertures ($A_1 = 38.4 \text{ mm}^2$, $A_2 = 0.79 \text{ mm}^2$, and $A_3 = 0.032 \text{ mm}^2$) to optimize required angular sensitivity or collection efficiency. These apertures are approximately 550 mm from the illuminated area of the sample. A lens (L) is positioned behind the apertures to focus the sample plane onto a manually adjustable iris field stop (FS). A linear retarder (WP) (currently $\lambda/2$) is mounted onto a computer controlled rotation stage (ROT). A Glan-Thompson polarizer (POL) mounted onto a manual rotation stage follows the retarder; during measurements, the polarizer is maintained fixed. After passing through the field stop, the light is collected in an integrating sphere (IS). The integrating sphere has two output ports, onto which two detectors, a silicon photodiode (SiPD) and a photomultiplier tube (PMT), are mounted. The PMT has a manual shutter to prevent exposure to excessive light levels. This receiver design has a linear dynamic range of about 15 orders of magnitude (in units of sr^{-1}), a maximum angular resolution of 0.02° , and a polarization extinction factor of about 10^4 . The instrument signature is Rayleigh-scattering-limited within about 1° from the specular direction.^{14,16}

One drawback of this instrument design is that the specular beam is not effectively captured. The field of view of the receiver includes not only the sample, but also part of the surrounding laboratory, which can be illuminated by scattered light from the uncaptured specular beam. If the surroundings are entirely absorbing (painted black), and

the field of view is sufficiently small, then this drawback may not be serious. In this instrument, the FS limits the field of view at the sample position to be adjustable from 3 mm to 38 mm, and is most typically set to about 10 mm. The laser sources must also be kept to a power that will not physically damage the surroundings, and adequate precautions must be taken to guarantee the eye safety of personnel.

The polarizers and retarders are aligned using a procedure that guarantees that their axes are either parallel or perpendicular with respect to the goniometer axes. Initially, the receiver polarizer and the two retarders are removed from the system. A sample is placed in the sample holder and rotated into Brewster's angle θ_B ($\alpha = \theta_B$ and $\beta = 0$). The incident polarizer is then adjusted to minimize the reflected signal. Next, the sample is removed, and the receiver is positioned in the "straight-through" position ($\delta = 180^\circ$). At this time, the receiver polarizer is mounted in its holder and adjusted to minimize the signal passing to the detector. Finally, the two retarders are mounted consecutively on their rotation stages, each being adjusted to minimize the signal before mounting the other. In this manner, the incident light is *p*-polarized and the detector only detects *s*-polarized reflected light, when the instrument is performing in-plane measurements ($\beta = 0$). Other in-out polarization combinations are obtained by rotating the retarders, using this alignment point as a reference.

III. TRANSFORMATIONS

The sample reference frame coordinate system is shown in Fig. 4. It is the purpose of Sec. III.A to derive the expressions necessary to convert the goniometer angles, α , β , γ , and δ , to the sample coordinate system angles, θ_i , ϕ_i , θ_r , and ϕ_r . In the following section, Sec. III.B, the transformation will be inverted. Finally, the relationships between

the polarization axes in the sample and laboratory coordinate systems will be derived in Sec. III.C.

A. Converting Goniometer Angles to Sample Reference Frame Angles

We begin by defining two coordinate systems, using unit basis vectors $\{\hat{x}', \hat{y}', \hat{z}'\}$ (see Fig. 2), which are fixed with respect to the laboratory, and $\{\hat{x}, \hat{y}, \hat{z}\}$ (see Fig. 4), which are fixed with respect to the sample. When $\alpha = \beta = \gamma = 0$, the two bases are identical. By applying a rotation of angle γ about \hat{z}' , followed by a rotation of angle β about \hat{x}' , and lastly, a rotation of angle α about \hat{y}' , the two bases can be related for arbitrary orientation of the sample holder:

$$\hat{x} = (\cos \alpha \cos \gamma - \sin \alpha \sin \beta \sin \gamma) \hat{x}' - (\cos \beta \sin \gamma) \hat{y}' - (\cos \gamma \sin \alpha + \cos \alpha \sin \beta \sin \gamma) \hat{z}', \quad (3a)$$

$$\hat{y} = (\cos \gamma \sin \alpha \sin \beta + \cos \alpha \sin \gamma) \hat{x}' + (\cos \beta \cos \gamma) \hat{y}' + (\cos \alpha \cos \gamma \sin \beta - \sin \alpha \sin \gamma) \hat{z}', \quad (3b)$$

and

$$\hat{z} = (\cos \beta \sin \alpha) \hat{x}' - (\sin \beta) \hat{y}' + (\cos \alpha \cos \beta) \hat{z}'. \quad (3c)$$

From Fig. 2, it can be seen that the incoming propagation direction is

$$\hat{k}_i = -\hat{z}', \quad (4a)$$

while for an arbitrary δ the detection direction is given by

$$\hat{k}_r = \hat{x}' \sin \delta + \hat{z}' \cos \delta. \quad (4b)$$

It is now straightforward to determine the polar and azimuthal angles of the incoming and outgoing light. For the polar angles θ_i and θ_r , the inner products of $-\hat{k}_i$ and \hat{k}_r with the surface normal \hat{z} , respectively, give the cosines of θ_i and θ_r , so that

$$\theta_i = \arccos(-\hat{k}_i \cdot \hat{z}) = \arccos(\cos \alpha \cos \beta) \quad (5a)$$

and

$$\theta_r = \arccos(\hat{\mathbf{k}}_r \cdot \hat{\mathbf{z}}) = \arccos(\cos \beta \sin \alpha \sin \delta + \cos \alpha \cos \beta \cos \delta). \quad (5b)$$

For the azimuthal angles, ϕ_i and ϕ_r , we use the projections of $\hat{\mathbf{k}}_i$ and $\hat{\mathbf{k}}_r$ onto $\hat{\mathbf{x}}$ and $\hat{\mathbf{y}}$:

$$\begin{aligned} \phi_i &= \arctan(-\hat{\mathbf{k}}_i \cdot \hat{\mathbf{x}}, -\hat{\mathbf{k}}_i \cdot \hat{\mathbf{y}}) \\ &= \arctan(-\cos \gamma \sin \alpha - \cos \alpha \sin \beta \sin \gamma, \cos \alpha \cos \gamma \sin \beta - \sin \alpha \sin \gamma), \end{aligned} \quad (6a)$$

and

$$\begin{aligned} \phi_r &= \arctan(\hat{\mathbf{k}}_r \cdot \hat{\mathbf{x}}, \hat{\mathbf{k}}_r \cdot \hat{\mathbf{y}}) \\ &= \arctan[-\cos \delta (\cos \gamma \sin \alpha - \cos \alpha \sin \beta \sin \gamma) + \\ &\quad \sin \delta (\cos \alpha \cos \gamma - \sin \alpha \sin \beta \sin \gamma), \\ &\quad \sin \delta (\cos \gamma \sin \alpha \sin \beta + \cos \alpha \sin \gamma) + \\ &\quad \cos \delta (\cos \alpha \cos \gamma \sin \beta - \sin \alpha \sin \gamma)], \end{aligned} \quad (6b)$$

where the function $\arctan(a, b)$ returns the complex argument of $a + ib$.

B. Converting Sample Reference Frame Angles to Goniometer Angles

In Sec. III.A, we have calculated the sample-relative scattering angles when the goniometer angles are known. However, it is often common to ask the opposite question, since one is generally interested in controlling the goniometer with sample-specific angles (θ_i , ϕ_i , θ_r , and ϕ_r).

Recognizing that δ is the angle subtended by the incoming and outgoing beams, we can readily solve for it. Working in a coordinate system natural to the sample it is

apparent from the standard formulae for polar-rectilinear transformations that

$$-\hat{\mathbf{k}}_i = \sin \theta_i \cos \phi_i \hat{\mathbf{x}} + \sin \theta_i \sin \phi_i \hat{\mathbf{y}} + \cos \theta_i \hat{\mathbf{z}} \quad (7a)$$

and

$$\hat{\mathbf{k}}_r = \sin \theta_r \cos \phi_r \hat{\mathbf{x}} + \sin \theta_r \sin \phi_r \hat{\mathbf{y}} + \cos \theta_r \hat{\mathbf{z}}. \quad (7b)$$

Again, we use the inner product to calculate the cosine of the subtended angle,

$$\begin{aligned} \cos \delta &= \hat{\mathbf{k}}_i \cdot \hat{\mathbf{k}}_r \\ &= \cos \theta_i \cos \theta_r + \cos \phi_i \cos \phi_r \sin \theta_i \sin \theta_r + \sin \phi_i \sin \phi_r \sin \theta_i \sin \theta_r. \end{aligned} \quad (8)$$

Eq. 5(a) allows us to eliminate β from Eq. 5(b) and solve for the rotation of the sample about the vertical axis of the goniometer, α :

$$\alpha = \arctan [(\cos \theta_r - \cos \theta_i \cos \delta) / (\cos \theta_i \sin \delta)]. \quad (9)$$

By recognizing that $\hat{\mathbf{y}}'$ is a unit vector pointing in the vertical direction in the laboratory, that

$$\hat{\mathbf{y}}' = -(\hat{\mathbf{k}}_i \times \hat{\mathbf{k}}_r) / |\hat{\mathbf{k}}_i \times \hat{\mathbf{k}}_r|, \quad (10)$$

that $\hat{\mathbf{z}}$ is the surface normal, and that $\hat{\mathbf{y}}'$ and $\hat{\mathbf{z}}$ are both perpendicular to the β axis, β can be derived from

$$\begin{aligned} \sin \beta &= \hat{\mathbf{y}}' \times \hat{\mathbf{z}} \\ &= \sin(\phi_r - \phi_i) \sin \theta_r \sin \theta_i / \sin \delta, \end{aligned} \quad (11)$$

where we have used $\sin \delta = |\hat{\mathbf{k}}_i \times \hat{\mathbf{k}}_r|$. The easiest way to solve for the rotation of the sample about its normal, γ , is to calculate ϕ'_i or ϕ'_r for $\gamma = 0$ and then set $\gamma = \phi_r - \phi'_r = \phi_i - \phi'_i$. Therefore, from Eq. 6(a),

$$\gamma = \phi_i - \arctan(-\sin \alpha, \cos \alpha \sin \beta). \quad (12)$$

The expressions in Eqs. 9 and 11 lead to intermediate singularities when $\delta = 0$ (retro-reflection), for which $\alpha = \theta_i$ and $\beta = 0$.

C. The Polarization Coordinates

We will work under the assumption that the most natural basis set for studying the polarization of scattered light contains the $\hat{\mathbf{s}}$ and $\hat{\mathbf{p}}$ vectors associated with the plane of incidence for the incident light and the plane of exitance for the exiting light. The planes of incidence and exitance are defined by the sample normal and $\hat{\mathbf{k}}_i$ and $\hat{\mathbf{k}}_r$, respectively. The basis vectors used to describe the polarization that are most natural in the laboratory frame are therefore given by

$$\hat{\mathbf{s}}'_i = \hat{\mathbf{y}}', \quad (13a)$$

and

$$\hat{\mathbf{p}}'_i = \hat{\mathbf{x}}', \quad (13b)$$

for the incident light, and

$$\hat{\mathbf{s}}'_r = \hat{\mathbf{y}}' \quad (13c)$$

and

$$\hat{\mathbf{p}}'_r = -\hat{\mathbf{x}}' \cos \delta + \hat{\mathbf{z}}' \sin \delta, \quad (13d)$$

for the scattered light. When measuring the polarization properties of out-of-plane optical scattering, we must be aware that the coordinate system natural to the sample will require rotation of the incoming and outgoing polarization analyzers so that they remain in the sample coordinate system. Therefore, we define a new set of basis vectors

$$\hat{\mathbf{s}}_i = (\hat{\mathbf{k}}_i \times \hat{\mathbf{z}}) / |\hat{\mathbf{k}}_i \times \hat{\mathbf{z}}|, \quad (14a)$$

and

$$\hat{\mathbf{p}}_i = \hat{\mathbf{k}}_i \times \hat{\mathbf{s}}_i, \quad (14b)$$

for the incident light, and

$$\hat{\mathbf{s}}_r = (\hat{\mathbf{k}}_r \times \hat{\mathbf{z}}) / |\hat{\mathbf{k}}_r \times \hat{\mathbf{z}}|, \quad (14c)$$

and

$$\hat{\mathbf{p}}_s = \hat{\mathbf{k}}_r \times \hat{\mathbf{s}}_r \quad (14d)$$

for the scattered light. It can be verified that the four sets of unit vectors, $\{\hat{\mathbf{s}}_i, \hat{\mathbf{p}}_i, \hat{\mathbf{k}}_i\}$, $\{\hat{\mathbf{s}}_r, \hat{\mathbf{p}}_r, \hat{\mathbf{k}}_r\}$, $\{\hat{\mathbf{s}}'_i, \hat{\mathbf{p}}'_i, \hat{\mathbf{k}}_i\}$, and $\{\hat{\mathbf{s}}'_r, \hat{\mathbf{p}}'_r, \hat{\mathbf{k}}_r\}$, form right-handed orthogonal coordinate systems. Furthermore, for measurements in the plane of incidence, the primed polarization coordinates and the unprimed polarization coordinates are the equivalent. We need to know the angle ψ_i that $\hat{\mathbf{s}}_i$ and $\hat{\mathbf{p}}_i$ are rotated with respect to $\hat{\mathbf{s}}'_i$ and $\hat{\mathbf{p}}'_i$, and the angle ψ_r that $\hat{\mathbf{s}}_r$ and $\hat{\mathbf{p}}_r$ are rotated with respect to $\hat{\mathbf{s}}'_r$ and $\hat{\mathbf{p}}'_r$. As usual, these angles can be determined by inner products with each other:

$$\cos \psi_i = \hat{\mathbf{s}}'_i \cdot \hat{\mathbf{s}}_i, \quad (15a)$$

$$\sin \psi_i = \hat{\mathbf{p}}'_i \cdot \hat{\mathbf{s}}_i, \quad (15b)$$

$$\cos \psi_r = \hat{\mathbf{s}}'_r \cdot \hat{\mathbf{s}}_r, \quad (15c)$$

and

$$\sin \psi_r = \hat{\mathbf{p}}'_r \cdot \hat{\mathbf{s}}_r. \quad (15d)$$

Using Eq. 3 and 4, the angles ψ_i and ψ_r can be readily shown to be

$$\psi_i = \arctan(\cos \psi_i, \sin \psi_i) = \arctan(-\sin \beta, \cos \beta \sin \alpha), \quad (16a)$$

and

$$\psi_r = \arctan(\cos \psi_r, \sin \psi_r) = \arctan[\sin \beta, \cos \beta \sin(\alpha - \delta)]. \quad (16b)$$

IV. NON-HANDED POLARIMETRIC MEASUREMENTS

Although the description of the instrument and the transformations described in the preceding sections are relevant to full polarimetric measurements of surface scatter, recent results have indicated that a substantial amount of information can be found from just the non-handed elements of the Mueller matrix.^{17,18} Furthermore, measurements of the full 4×4 Mueller matrix are often prone to large uncertainties;¹⁹ reducing the number of parameters being sought can help to reduce these uncertainties. Measurements of the full Mueller matrix are described in detail elsewhere and do not need repeating here.²⁰ In this section, details associated with the measurement of the non-handed 3×3 Mueller matrix are reviewed.

A. Bidirectional Ellipsometry Parameters

It is often useful to condense the terms in the Mueller matrix from sixteen to a more manageable number. Previous work has demonstrated that specific incident polarizations (usually p) are particularly useful for distinguishing between different sources of scatter near a surface, especially when viewing the sample out of the plane of incidence.^{6,7,17,18} Although one can present the Stokes parameters for the scattered light for a fixed incident polarization, it has been found to be particularly useful to present the results using bidirectional ellipsometry parameters, for which η represents the principle angle of the polarization and P_L represents the degree of linear polarization. For a number of scattering mechanisms (for example, scatter of p -polarized light from microroughness of non-metallic materials), $P_L \sim 1$, so that the value of η essentially describes the polarization.

The angle $\eta^{(p)}$ [$\eta^{(s)}$] that the principle axis of the polarization ellipse makes with respect to the \hat{s} axis when the incident light is p -polarized (s -polarized) can be determined from the Mueller matrix to be²¹

$$\eta^{(p)} = \arctan(M_{21} - M_{22}, M_{31} - M_{32})/2 \quad (17a)$$

and

$$\eta^{(s)} = \arctan(M_{21} + M_{22}, M_{31} + M_{32})/2. \quad (17b)$$

As a measure of the degree to which the light is linearly polarized, the degree of linear polarization is

$$P_L = (f_{\max} - f_{\min})/(f_{\max} + f_{\min}) \quad (18)$$

where f_{\max} and f_{\min} are the maximum and minimum scattered light signals measured as an analyzing linear polarizer in front of the detector is rotated. For linearly polarized light, $P_L = 1$, and for purely depolarized light or completely circularly polarized light, $P_L = 0$. From the Mueller matrix elements, the degrees of linear polarization for p - and s -polarized incident light are

$$P_L^{(p)} = [(M_{21} - M_{22})^2 + (M_{31} - M_{32})^2]^{1/2}/(M_{11} - M_{12}) \quad (19a)$$

and

$$P_L^{(s)} = [(M_{21} + M_{22})^2 + (M_{31} + M_{32})^2]^{1/2}/(M_{11} + M_{12}), \quad (19b)$$

respectively. By placing attention on the principle axis of the polarization ellipse, certain issues can be ignored. Foremost of these is the scattering from other objects in the room which are illuminated by the specular beam. This light is most likely to be highly depolarized, and therefore will have little effect on the measurement of η .

The complex ratio of the p -polarized component to the s -polarized component is often expressed as $\tan(\Psi) \exp(i\Delta)$. If we assume (and this is often not correct) that there

is no depolarization, then we can relate the bidirectional ellipsometry parameters η and P_L and the standard ellipsometry parameters Δ and Ψ :

$$\tan(2\eta) = -\tan(2\Psi) \cos \Delta \quad (20a)$$

and

$$(1 - P_L^2)^{1/2} = \sin(2\Psi) \sin \Delta. \quad (20b)$$

Eqs. 20(a-b) can be inverted to yield

$$\sin^2 \Delta = (1 - P_L^2)[1 + \tan^2(2\eta)]/[1 + \tan^2(2\eta) - P_L^2]. \quad (21b)$$

and

$$\Psi = \arctan[-\sin(2\eta) \cos \Delta, \cos(2\eta)]/2. \quad (21a)$$

B. The $\omega:4\omega$ Method

Measurements of the non-handed 3×3 Mueller matrix using half-wave retarders before and after the sample is straightforward using the techniques outlined by Azzam²⁰ for determining the full 4×4 Mueller matrix with quarter-wave retarders. The retarders are rotated, that on the receiver at four times the rate of that on the source, to yield a signal as a function of retarder rotation. The signal can be shown to be given by

$$\begin{aligned} S_{\omega 4:\omega}(\xi) = & M_{11} - M_{12} \cos(4\xi) - M_{22} \cos(12\xi)/2 - M_{33} \cos(12\xi)/2 \\ & + M_{21} \cos(16\xi) - M_{22} \cos(20\xi)/2 + M_{33} \cos(20\xi)/2 - M_{13} \sin(4\xi) \\ & + M_{23} \sin(12\xi)/2 - M_{32} \sin(12\xi)/2 + M_{31} \sin(16\xi) - M_{23} \sin(20\xi)/2 \\ & + M_{32} \sin(20\xi)/2, \end{aligned} \quad (22)$$

where ξ is the rotation angle of the input retarder. Eq. 22 is of the form

$$S(\xi) = \sum_j [c_j \cos(j\xi) + s_j \sin(j\xi)], \quad (23)$$

so that a Fourier analysis of the signal will yield the values of c_j and s_j . The Mueller matrix elements of the sample can be determined from the c_j and s_j to be:

$$M = \begin{pmatrix} c_0 & -c_4 & -s_4 & \text{n.d.} \\ c_{16} & -c_{12} - c_{20} & s_{12} - s_{20} & \text{n.d.} \\ s_{16} & -s_{12} + s_{20} & -c_{12} + c_{20} & \text{n.d.} \\ \text{n.d.} & \text{n.d.} & \text{n.d.} & \text{n.d.} \end{pmatrix}. \quad (24)$$

Since half-wave retarders are used, the terms in the fourth row and fourth column are not determined (n.d.). In practice, sixteen measurements are performed, while the incident retarder is rotated from 0° to $90^\circ \times (15/16) = 84.375^\circ$, and while the receiver retarder is rotated from 0° to $360^\circ \times (15/16) = 337.5^\circ$. The sixteen measurements are then Fourier transformed to yield the c_j and s_j .

There may exist errors in the retardance of the polarizers of δ_1 and δ_2 for the first and second retarders, respectively. We can determine some of the effects these errors may have on the measurement of M by calculating the expected signal like that for Eq. 22, and applying the results of Eqs. 23 and 24 and assuming that M is the unit matrix. Although the general result is rather complicated, we can expand the result in powers of δ_1 and δ_2 , and arrive at the lowest-order result

$$M = \begin{pmatrix} 1 & \delta_2^2/4 & 0 & \text{n.d.} \\ -\delta_1^2/4 & 1 - \delta_1^2/4 - \delta_2^2/4 & 0 & \text{n.d.} \\ 0 & 0 & 1 - \delta_1^2/4 - \delta_2^2/4 & \text{n.d.} \\ \text{n.d.} & \text{n.d.} & \text{n.d.} & \text{n.d.} \end{pmatrix}. \quad (25)$$

Similarly, one can calculate the $\eta^{(p)}$ and $P_L^{(p)}$ that is expected when one measures a high quality polarizer as a function of the rotation angle of the polarizer, θ . One arrives at the result that no error is created in $\eta^{(p)}$, and that the measured degree of linear polarization is

$$P_L^{(p)} = (4 - \delta_2^2)/[4 + \delta_2^2 \cos(2\theta)]. \quad (26)$$

C. The $\omega:3\omega$ Method

The same measurement may be carried out with the receiver retarder rotating at three times the rate of the incident retarder. In this case, the signal is given by

$$\begin{aligned} S_{\omega:3\omega}(\xi) = & M_{11} - M_{12} \cos(4\xi) - M_{22} \cos(8\xi)/2 - M_{33} \cos(8\xi)/2 \\ & + M_{21} \cos(12\xi) - M_{22} \cos(16\xi)/2 + M_{33} \cos(16\xi)/2 - M_{13} \sin(4\xi) \\ & + M_{23} \sin(8\xi)/2 - M_{32} \sin(8\xi)/2 + M_{31} \sin(12\xi) - M_{23} \sin(16\xi)/2 \\ & - M_{32} \sin(16\xi)/2, \end{aligned} \quad (27)$$

from which the Mueller matrix can be found to be

$$M = \begin{pmatrix} c_0 & -c_4 & -s_4 & \text{n.d.} \\ c_{12} & -c_8 - c_{16} & s_8 - s_{16} & \text{n.d.} \\ s_{12} & -s_{16} - s_8 & -c_8 + c_{16} & \text{n.d.} \\ \text{n.d.} & \text{n.d.} & \text{n.d.} & \text{n.d.} \end{pmatrix}. \quad (28)$$

Similar analysis of errors can be carried out for the $\omega:3\omega$ method as for the $\omega:4\omega$ method. A measurement of the unit Mueller matrix will yield

$$M = \begin{pmatrix} 1 & \delta_2^2/4 - \delta_1\delta_2/2 & 0 & \text{n.d.} \\ -\delta_1^2/4 & 1 - (\delta_1 - \delta_2)^2/4 & 0 & \text{n.d.} \\ 0 & 0 & 1 - (\delta_1 - \delta_2)^2/4 & \text{n.d.} \\ \text{n.d.} & \text{n.d.} & \text{n.d.} & \text{n.d.} \end{pmatrix}. \quad (29)$$

Once again, measurement of a polarizer yields no error for $\eta^{(p)}$, and a measured degree of linear polarization the same as Eq. 26.

D. Uncertainties

A series of consecutive measurements of the Mueller matrix with no sample present should yield the unity matrix, and an estimate of the random and systematic uncertainties in Mueller matrix measurements. Such a measurement was carried out with eighty measurements using the $\omega:4\omega$ method and yielded

$$\begin{pmatrix} 1 & (5.2 \pm 1.7) \times 10^{-4} & (1.6 \pm 0.7) \times 10^{-4} & \text{n.d.} \\ (8.1 \pm 0.9) \times 10^{-4} & 0.9995 \pm 0.0001 & (4.0 \pm 0.9) \times 10^{-4} & \text{n.d.} \\ (-4.2 \pm 1.7) \times 10^{-4} & (2.2 \pm 0.3) \times 10^{-3} & 1.0008 \pm 0.0001 & \text{n.d.} \\ \text{n.d.} & \text{n.d.} & \text{n.d.} & \text{n.d.} \end{pmatrix},$$

where we have normalized the elements to M_{11} . The uncertainties quoted above are the standard deviation of the eighty measurements, and therefore are an indication of the random uncertainty for a single measurement. The deviation of this matrix from the unity matrix is an indication of systematic errors in the system. Considering horizontal linearly polarized light, these measurements yielded values of $|\eta - \eta^{\text{expect}}| = 0.08^\circ$ and $|P_L - P_L^{\text{expect}}| = 0.0007$, with standard deviations of $\sigma_\eta = 0.01^\circ$ and $\sigma_{P_L} = 0.0003$, respectively.

As another test of systematic uncertainties that can occur in measurements of the polarization state, the Mueller matrix of a Glan-Taylor polarizer was measured in transmission as a function of the polarizer rotation angle θ . Each measured Mueller matrix was then transformed back into that for the unrotated polarizer. These results yielded standard deviations of $\sigma_\eta = 0.2^\circ$ and $\sigma_{P_L} = 0.005$. The mean value of P_L deviated from its expected value of unity by 0.001. The measured polarization angle η and the degree

of linear polarization therefore typically has expanded uncertainties ($k = 2$) of 0.4° and 0.01, respectively, when $P_L \sim 1$.

None of the errors are consistent with those arising from retardance errors in the retarders as calculated in Sec. IV. Other systematic errors can result from residual birefringence in the lenses used in the spatial filter and in the receiver, reflection from the focussing primary mirror, wobble during rotation of the retarders, and small degrees of inhomogeneity²² (non-orthogonality of the eigenpolarizations) of the retarders.

These uncertainties are assumed to be in addition to the random uncertainties associated with electronic noise, laser fluctuations, and depolarization. The first two of these can be estimated by measuring a standard deviation of several measurements of each in-out retarder combination. The uncertainty in a particular variable, be it a matrix element, η , or P_L , can most easily be estimated by Monte Carlo sampling over the variation of the measured quantities. These random uncertainties contribute to the total uncertainty in a root-sum-squared fashion.

When the measured light has P_L less than unity, the uncertainty can have a contribution larger than that estimated by the above means. If the light is completely polarized ($P = 1$), then no additional uncertainty is incurred. However, if the light has some depolarization (and the light is monochromatic), then the polarization state of the light fluctuates from one direction to another, being completely polarized in any differential direction. In fact, speckle-like fluctuations of the polarization state indicate the presence of depolarization.^{23–27} For measurements presented herein, we will not consider further the uncertainties associated with polarization speckle, being that these uncertainties are not associated with the instrument but with randomness associated with the sample.

V. RESULTS

In this section, we illustrate the use of the system by presenting 3×3 Mueller matrix measurements of a titanium nitride film grown on a silicon wafer. The measurements were carried out with incident and scattering angles of $\theta_i = \theta_r = 60^\circ$ and with a wavelength $\lambda = 532$ nm. The Mueller matrix is then measured as a function of the azimuthal scattering angle ϕ_r . Therefore, the probed scattering directions map out a cone in space, beginning in the specular direction (for $\phi_r = 0^\circ$) and ending in the retroreflection direction (for $\phi_r = 180^\circ$). All of the measured scattering directions, except those in the extremes, are out of the plane of incidence. In this arrangement, where $\theta_i = \theta_r$, the spatial frequencies of roughness that are measured are given by the Bragg relation $f = 2 \sin \theta_i \sin(\phi_r/2)/\lambda$.

Figure 5 shows the results of the 3×3 Mueller matrix measurements from the titanium nitride layer. In the upper graph is the unpolarized BRDF, M_{11} , which varies more than an order of magnitude in the angular range shown. In fact, just to the left of the data (near the specular direction, $\phi_r = 0^\circ$), the value of M_{11} rises many orders of magnitude; data are not shown near the specular beam since the focus of this paper is on the polarimetry, and little interesting occurs there.

In the lower graph of Fig. 5 are shown the other elements of the 3×3 Mueller matrix, normalized to M_{11} . Despite the strong dependence of M_{11} on angle, the normalized Mueller matrix elements vary smoothly from one angle to the next. The curves in Fig. 5 are predictions of first-order vector perturbation theory for scattering from surface roughness,⁶ assuming a complex index of refraction of $\tilde{n} = 1.80 + 1.28i$. The agreement between the theory and experiment appear to be very good.

In Fig. 6, the bidirectional ellipsometry parameters $\eta^{(p)}$ and $P_L^{(p)}$ are shown for the titanium nitride sample. Once again, the theoretical predictions for surface roughness, shown as curves, model the data very well. Since the model does not have any depolarizing mechanisms, the appearance of $P_L^{(p)} < 1$ for both the theory and the experiment give strong evidence that the scattered light has a significant degree of circular polarization.

Figure 7 shows the data presented in terms of the standard ellipsometric parameters Δ and Ψ , for p -polarized incident light. The agreement between the theory and experiment does not appear as good as that for the other parameters previously presented. The determination of Δ and Ψ , given in Eqs. 20 and 21, assume that no depolarization has occurred. Although the depolarization is probably very small, the solutions to Δ and Ψ are rather sensitive to the value of $1 - P_L$. Systematic errors discussed above can cause the measured value of P_L to deviate from unity, even when the light is known to be linearly polarized. For these reasons, we avoid using the parameters Δ and Ψ , and instead use the more directly measured parameters η and P_L .

Further analysis of the data and presentations of data for other samples have been relegated to other publications.^{7,17,18,28} The scattering of light out of the plane of incidence has significant structure that often enables one to identify the source of scattered light, be it from microroughness, particles, or subsurface defects. When analyzed in terms of the bidirectional ellipsometry parameters, different scattering mechanisms can be readily identified. Although full in-plane Mueller matrix measurements can be used to discriminate between different scattering mechanisms, the interpretation of the data has been found to be more difficult. The analysis of the instrument presented in this paper should allow out-of-plane scattering measurements to be more readily available in the future.

ACKNOWLEDGEMENTS

The authors would like to thank Charles Weber of Sematech for supplying the titanium nitride sample.

FIGURE CAPTIONS

FIGURE 1 An overall schematic of the goniometric optical scatter instrument (GOSI). (Not to scale.)

FIGURE 2 A schematic diagram of GOSI's goniometer, showing the laboratory coordinate system basis vectors (\hat{x}' , \hat{y}' , and \hat{z}'), and the goniometer angles (α , β , γ , and δ).

FIGURE 3 A schematic of the instrument's receiver (not to scale): A_1 , A_2 , and A_3 are solid-angle-limiting apertures, mounted on a translation stage T; L is a lens; WP is a $\lambda/2$ retarder, mounted on a rotation stage ROT; POL is a polarizer; FS is an adjustable iris field stop; IS is an integrating sphere; PMT is a photomultiplier tube; SH is a manual shutter; and SiPD is a silicon photodiode.

FIGURE 4 The sample coordinate system.

FIGURE 5 The measured 3×3 Mueller matrix elements as a function of ϕ_r for $\theta_i = \theta_r = 60^\circ$ for an optically thick titanium nitride film grown on silicon. The upper graph shows the BRDF, M_{11} , while the lower graph shows the other eight normalized to M_{11} . The solid curves in the lower graph represent the predictions of first-order vector perturbation theory.

FIGURE 6 The bidirectional ellipsometry parameters $P_L^{(p)}$ and $\eta^{(p)}$ derived from the data in Fig. 5.

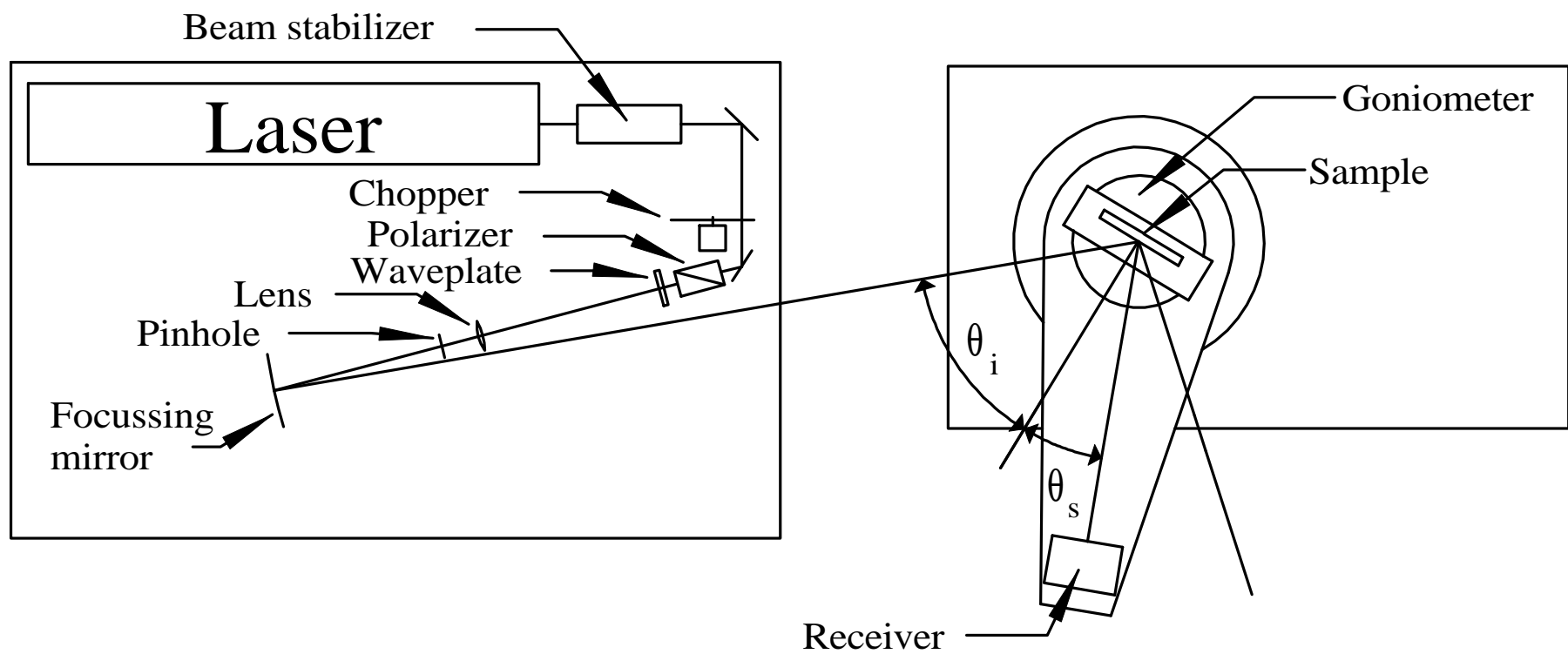
FIGURE 7 The standard ellipsometry parameters Δ and Ψ for p -polarized incident light, derived from the data in Fig. 5.

REFERENCES

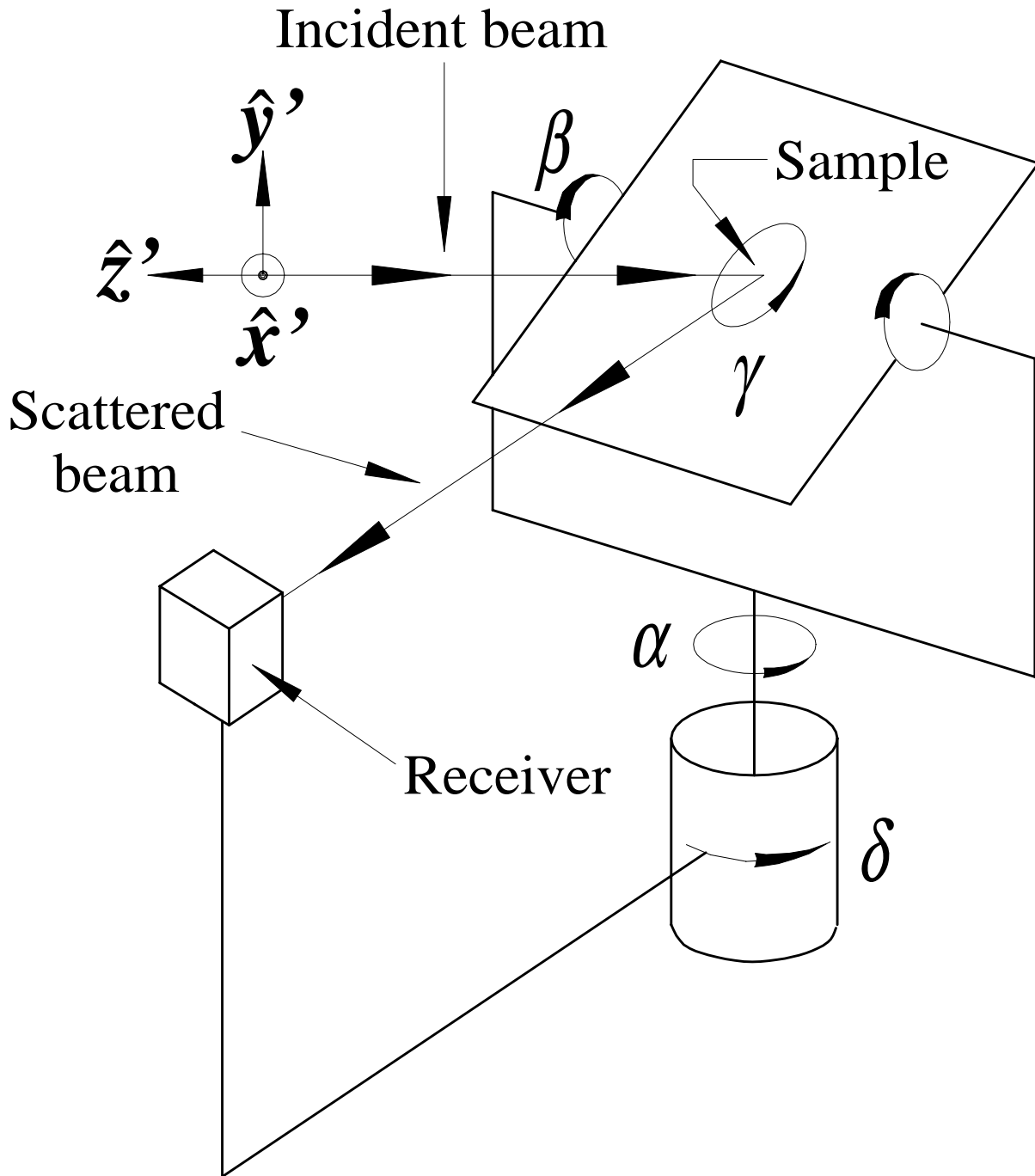
- [1] J. C. Stover, *Optical Scattering: Measurement and Analysis*, (SPIE Optical Engineering Press, Bellingham, WA, 1995).
- [2] F. E. Nicodemus, J. C. Richmond, J. J. Hsia, I. W. Ginsberg, and T. Limperis, “Geometrical Considerations and Nomenclature for Reflectance,” NBS Monograph 160, National Bureau of Standards (Gaithersburg, 1977).
- [3] E. R. Méndez, A. G. Navarrete, and R. E. Luna, “Statistics of the polarization properties of one-dimensional randomly rough surfaces,” *J. Opt. Soc. Am. A* **12**, 2507–2516 (1995).
- [4] D. L. Jordan, G. D. Lewis, and E. Jakeman, “Emission polarization of roughened glass and aluminum surfaces,” *Appl. Opt.* **35**, 3583–3590 (1996).
- [5] S.-M. F. Nee, “Polarization of specular reflection and near-specular scattering by a rough surface,” *Appl. Opt.* **35**, 3570–3582 (1996).
- [6] T. A. Germer, “Angular dependence and polarization of out-of-plane optical scattering from particulate contamination, subsurface defects, and surface microroughness,” *Appl. Opt.* **36**, 8798–8805 (1997).
- [7] T. A. Germer, C. C. Asmail, and B. W. Scheer, “Polarization of out-of-plane scattering from microrough silicon,” *Opt. Lett.* **22**, 1284–1286 (1997).
- [8] R. E. Luna, “Scattering by one-dimensional random rough metallic surfaces in a conical configuration: several polarizations,” *Opt. Lett.* **21**, 1418–1420 (1996).
- [9] W. S. Bickel, R. R. Zito, and V. Iafelice, “Polarized Light Scattering From Metal Surfaces,” *J. Appl. Phys.* **61**, 5392–5398 (1987).
- [10] V. J. Iafelice, and W. S. Bickel, “Polarized Light-Scattering Matrix Elements for Select Perfect and Perturbed Optical Surfaces,” *Appl. Opt.* **26**, 2410–2415 (1987).

- [11] G. Videen, J.-Y. Hsu, W. S. Bickel, and W. L. Wolfe, "Polarized light scattered from rough surfaces," *J. Opt. Soc. Am. A* **9**, 1111-1118 (1992).
- [12] E. Bahar, and M. A. Fitzwater, "Like- and cross-polarized cross sections for random rough surfaces: theory and experiment," *J. Opt. Soc. Am. A* **2**, 2295-2303 (1985).
- [13] T. F. Schiff, M. W. Knighton, D. J. Wilson, F. M. Cady, J. C. Stover, and J. J. Butler, "Design review of a high accuracy UV to near IR scatterometer," in *Optical Scattering: Applications, Measurement, and Theory II*, J. C. Stover, ed., Proc. SPIE **1995**, 121-130 (1995).
- [14] C. C. Asmail, C. L. Cromer, J. E. Proctor, and J. J. Hsia, "Instrumentation at the National Institute of Standards and Technology for bidirectional reflectance distribution function (BRDF) measurements," in *Stray Radiation in Optical Systems III*, R. P. Breault, ed., Proc. SPIE **2260**, 52-61 (1994).
- [15] T. A. Germer, and C. C. Asmail, "A goniometric optical scatter instrument for bidirectional reflectance distribution function measurements with out -of-plane and polarimetry capabilities," in *Scattering and Surface Roughness*, Z.-H. Gu, and A. A. Maradudin, ed., Proc. SPIE **3141**, 220-231 (1997).
- [16] C. Asmail, J. Hsia, A. Parr, and J. Hoeft, "Rayleigh scattering limits for low-level bidirectional reflectance distribution function measurements," *Appl. Opt.* **33**, 6084-6091 (1994).
- [17] T. A. Germer, and C. C. Asmail, "Polarization of light scattered by microrough surfaces and subsurface defects," *J. Opt. Soc. Am. A* , ??-?? (submitted).
- [18] T. A. Germer, and C. C. Asmail, "Bidirectional ellipsometry and its application to the characterization of surfaces," in *Polarization: Measurement, Analysis, and Remote Sensing*, D. H. Goldstein, and R. A. Chipman, ed., Proc. SPIE **3121**, 173-182 (1997).

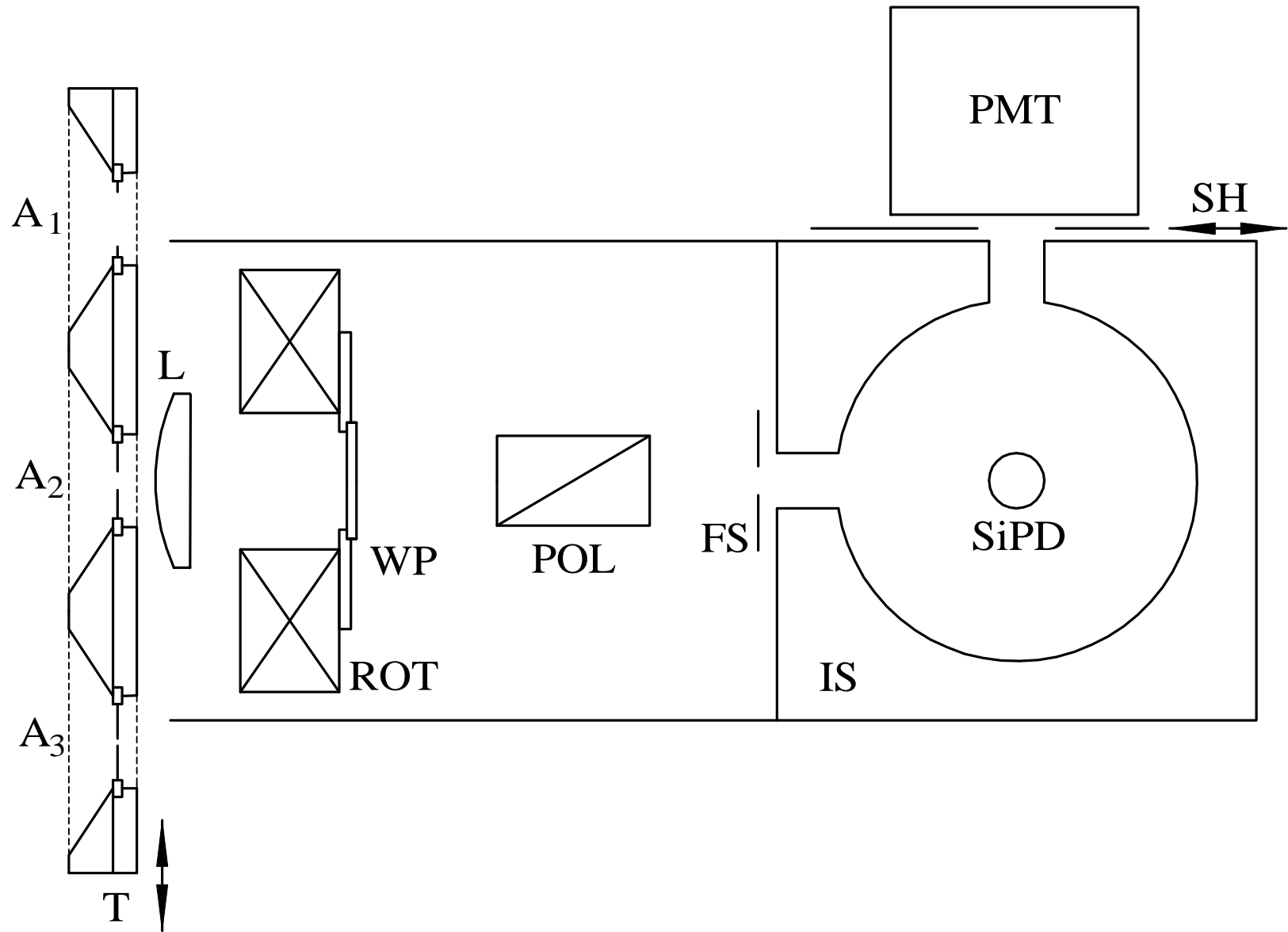
- [19] D. H. Goldstein, and R. A. Chipman, “Error analysis of a Mueller matrix polarimeter,” *J. Opt. Soc. Am. A* **7**, 693–700 (1990).
- [20] R. M. A. Azzam, “Photopolarimetric measurement of the Mueller matrix by Fourier analysis of a single detected signal,” *Opt. Lett.* **2**, 148–150 (1978).
- [21] R. A. Chipman, “Polarimetry,” in *Handbook of Optics, Vol. II*, Michael Bass, ed., pp. 22.1–37 (McGraw-Hill, New York, 1995).
- [22] S.-Y. Lu, and R. A. Chipman, “Homogeneous and inhomogeneous Jones matrices,” *J. Opt. Soc. Am. A* **11**, 766–773 (1994).
- [23] V. N. Kurashov, V. V. Marenko, and T. V. Molebnaya, “Conditional probability distribution of normalized Stokes parameters,” *Opt. Spektrosk. (USSR)* **71**, 998–1001 (1991).
- [24] P. F. Steeger, and A. F. Fercher, “Experimental investigation of the first-order statistics of Stokes parameters in speckle fields,” *Opt. Acta* **29**, 1395–1400 (1982).
- [25] A. R. Fercher, and P. F. Steeger, “First-order statistics of Stokes parameters in speckle fields,” *Opt. Acta* **28**, 443–448 (1981).
- [26] V. N. Kurashov, V. V. Marenko, and T. V. Molebnaya, “Statistics of normalized Stokes parameters of speckle fields,” *Opt. Spectrosk. (USSR)* **70**, 401–406 (1992).
- [27] P. F. Steeger, T. Asakura, K. Zocha, and A. F. Fercher, “Statistics of the Stokes parameters in speckle fields,” *J. Opt. Soc. Am. A* **1**, 677–682 (1984).
- [28] T. A. Germer, and B. W. Scheer, “Polarization of out-of-plane optical scatter from SiO₂ films grown on photolithographically-generated microrough silicon,” in *Scattering and Surface Roughness II*, Z.-H. Gu, and A. A. Maradudin, ed., Proc. SPIE **3426**, 160–168 (1998).



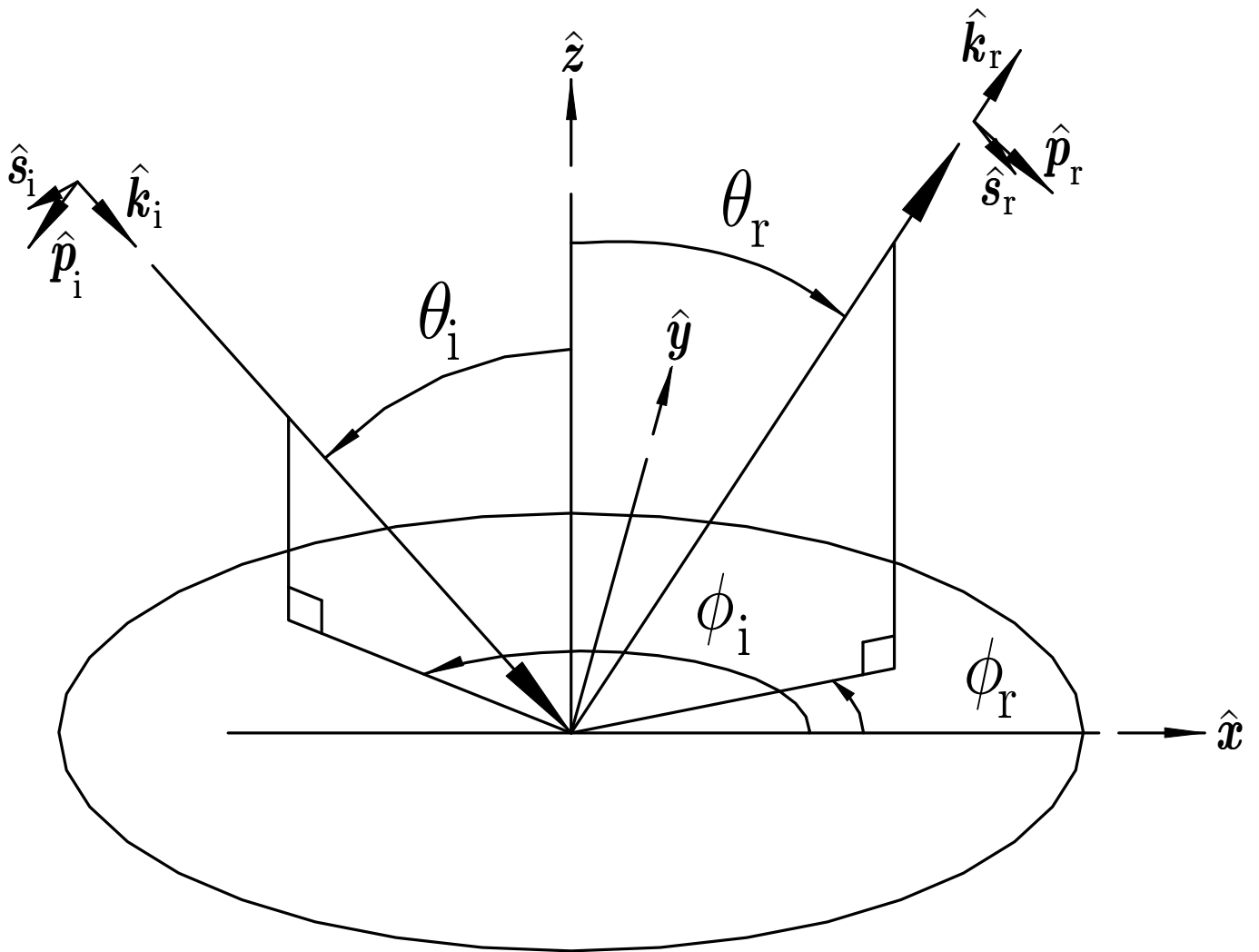
Germer and Asmail, Figure 1



Germer and Asmail, Figure 2



Germer and Asmail, Figure 3



Germer and Asmail, Figure 4

